Open camera or QR reader and
scan code to access this article
and other resources online.

ORIGINAL ARTICLE

Single-Step 3D Printing of Bio-Inspired Printable Joints Applied to a Prosthetic Hand

Haemin Lee,[1] JongHoo Park,[1] Brian Byunghyun Kang,[2] and Kyu-Jin Cho[1,3]

Abstract

Single-step 3D printing, which can manufacture complicated designs without assembly, has the potential to completely change our design perspective, and how 3D printing products, rather than printing static components, ready-to-use movable mechanisms become a reality. Existing 3D printing solutions are challenged by precision limitations, and cannot directly produce tightly mated moving surfaces. Therefore, joints must be designed with a sufficient gap between the components, resulting in joints and other mechanisms with imprecise motion. In this study, we propose a bio-inspired printable joint and apply it to a Single sTep 3D-printed Prosthetic hand (ST3P hand). We simulate the anatomical structure of the human finger joint and implement a cam effect that changed the distance between the contact surfaces through the elastic bending of the ligaments as the joint flexed. This bio-inspired design allows the joint to be single-step 3D printed and provides precise motion. The bio-inspired printable joint makes it possible for the ST3P hand to be designed as a lightweight (~ 255 g), low-cost ($\sim \$500$) monolithic structure with nine finger joints and manufactured via single-step 3D printing. The ST3P hand takes ~ 6 min to assemble, which is approximately one-tenth the assembly time of open-source 3D printed prostheses. The hand can perform basic hand tasks of activities of daily living by providing a pulling force of 48 N and grasp strength of 20 N. The simple manufacturing of the ST3P hand could help us take one step closer to realizing fully customized robotic prosthetic hands at low cost and effort.

Keywords: single-step 3D printing, bio-inspired joint, prosthetic hand, nonassembly mechanism

Introduction

ROBOTIC PROSTHETIC HANDS hold great promise for improving the quality of life by restoring high levels of hand function; therefore, they have been studied over several decades to improve users' quality of life. Recent research topics on prosthetic hands range from biomimetic or bio-inspired design, dexterous grasping capabilities,[1–4] a sense of touch restoration,[5] and intuitive control strategies via user intention detection and sensory feedback.[6–11] Meanwhile, commercial prosthetic hands have been focusing on their practicality such as an anthropomorphic appearance with individually actuated fingers and an opposable thumb, capable of making various postures and grasping different objects robustly.[12–14] How-

ever, the technological advances in recent studies and state-of-the-art commercial robotic prosthetic hands do not seem to provide a distinct general advantage over body-powered or cosmetic prostheses in performing activities of daily living (ADLs).[15]

One example can be found in the powered arm prosthetic race of Cybathlon in 2020; a participant with a simple four-fingered, body-powered prosthesis won first place by performing a series of tasks faster and more accurately than others with sophisticated robotic hands.[16–18] In fact, many hand amputees still rely on cosmetic or body-powered prosthetic hands rather than sophisticated robotic hands. One of the major factors contributing to the low acceptance rate of a robotic prosthetic hand, among other factors including a

[1]Biorobotics Laboratory, Department of Mechanical Engineering, Seoul National University, Seoul, Republic of Korea.
[2]Intelligent Robotics Laboratory, School of Intelligent Mechatronics Engineering, Sejong University, Seoul, Republic of Korea.
[3]Soft Robotics Research Center, Seoul National University, Seoul, Republic of Korea.

Opposite page: Concept art which illustrates the manufacturing process of the single-step 3D printable prosthetic hand (ST3P hand).
Image credit: J. J. -R. Song.

lack of sensory feedback and unnatural movements, is an insignificant functional advantage compared with its weight and cost.[15,19]

One way to reduce the weight and cost of a robotic prosthetic hand without functional degradation is to simplify the structural design of the multi-articulated mechanism. Implementing numerous finger joints in a prosthetic hand enables replicating the appearance and movements of the human hand, but, in turn, involves a complicated manufacturing process, increasing the cost and weight of the prosthetic hand.[12] As an alternative to mechanical joints, the compliance of soft structures has been utilized in prosthetics. Fabricated as monolithic structures, soft fingers or hands reduce the weight of the overall system, enable adaptive grasps, and provide simplicity of control.[20–30]

However, it is difficult for compliant joints to deliver the large range of motion required for a prosthetic finger or to withstand compressive loads because of the risk of plastic deformation.[31,32] Another approach for simplifying the structural design of a multi-articulated mechanism is to utilize a 3D-printed, preassembled joint.[33–36] Examples of so-called single-step 3D printable or nonassembly mechanisms that consist of 3D-printed, preassembled joints demonstrate the potential of fully autonomous robot manufacturing without an assembly process. By removing the components for joint assembly, such as bolts and bearings, a single-step 3D printing approach and its enabling design can reduce the weight and cost of the overall system.

However, the performance of existing single-step 3D printable mechanisms[33–39] is insufficient for applications that require precise transmission of force and displacement. This is mainly owing to the characteristics of 3D printing, such as rough surfaces and undesired fusion between thin gaps.[40–47] In traditional manufacturing processes, the pin and hole of a revolute joint are tightly mated using an assembly to provide precise rotational movement. However, when using single-step 3D printing, an appropriate gap size between the pin and hole should be designed to prevent undesired fusion. This sub-millimeter gap enables relative motion between the pin and hole; however, in return, it causes wobbling during joint movement.[48–55] Although attempts have been made to reduce the gap by changing the geometries of the pin and hole of the joint, a wobbling issue still exists.[56,57]

We propose a bio-inspired 3D printable joint that can be manufactured via single-step 3D printing and generates precise joint motion (Fig. 1). Inspired by the manner in which the cam effect works in human finger joints,[58–60] the joint was designed such that the gap changes as the joint bends. The joint exhibits a gap in the initial state, which is crucial for successful 3D printing and support removal. After printing, the gap was closed to ensure contact with the surface. Surface contact adds kinematic constraints to the joint, allowing for precise flexion and extension movements. The maximum allowable external moments for the proposed joint in the lateral and frontal directions were measured to be ~328 and 373 Nmm, respectively.

A periodic flexion–extension movement test demonstrated that the joint could withstand loads for 50,000 cycles exhibiting a robust fatigue life. We used this bio-inspired printable joint to create a Single-sTep 3D-printed Prosthetic hand (ST3P hand). The bio-inspired printable joint makes it possible for the finger joints, tendons, and palm of the ST3P hand to be designed as a monolithic structure that can be 3D printed in a single step without assembly. The ST3P hand is produced by 3D printing the structure, inserting actuators and electronics, and connecting the power source. The time required for assembly is approximately one-tenth that of open-source 3D printed prostheses.[38,39] The simplified assembly helps the ST3P hand to keep the price as low as possible so that people who actually need them can afford it.

The estimated total cost of a single ST3P hand was less than $500. To verify the mechanical characteristics of the ST3P hand, we performed several types of grasping tests including power, pinch, and object grasping. The test showed that the ST3P hand was capable of providing a pulling force of 48 N and a grasp strength of 20 N and successfully grasped multiple objects. We also propose various examples of single-step 3D-printed mechanisms designed by integrating bio-inspired printable joints (Fig. 2). We anticipate that our bio-inspired printable joint design and ST3P hand will become an example that enable the design and production of other customized prosthetic hands tailored to an ever-growing set of user requirements at low cost and effort.

Materials and Methods

Bio-inspired printable joint

The bio-inspired printable joint was designed as a monolithic structure consisting of a ligament, two cam surfaces, and two articulated surfaces (Fig. 1B). The ligament is a deformable, thin cantilever beam that generates the flexion and extension motions of the joint, whereas the cam and articulated surfaces, which are designed to be rigid, impose appropriate constraints on ligament deformation.

One of the main functions of the cam effect in the metacarpophalangeal (MCP) joint of the human hand is a change in the length of the collateral ligament (Fig. 1A).[58–60] When the joint angle increases, the ligament elongates and deforms as it is wound around the metacarpal head. Ligament elongation increases the internal contact force between the two bones, the metacarpal bone and the proximal phalanx, making the joint more stable. Conversely, the cam effect of the bio-inspired printable joint is designed not to cause ligament elongation but instead to reduce the gap between the articulated surfaces. There was a sufficient gap between the two articulated surfaces in the initial state of the joint. As the joint angle increases, the ligament is wound around the cam surfaces, the gap between the articulated surfaces gradually closes, and the articulated surfaces come into contact with each other. Based on whether there is contact between the articulated surfaces, two different states of the joint are defined: the postprinted state without contact and the functional state with contact. The gap in the postprinted state enables single-step 3D printing of the joint, preventing undesired material fusion between surfaces, and allowing the successful removal of support materials after 3D printing. Contact of the joint in the functional state imposes additional kinematic constraints on the joint, leading to precise flexion and extension motions (Fig. 1B).

Correlation between gap and involute curves

To realize the bio-inspired cam effect with single-step 3D printing, the correlation between the gap as a function of the
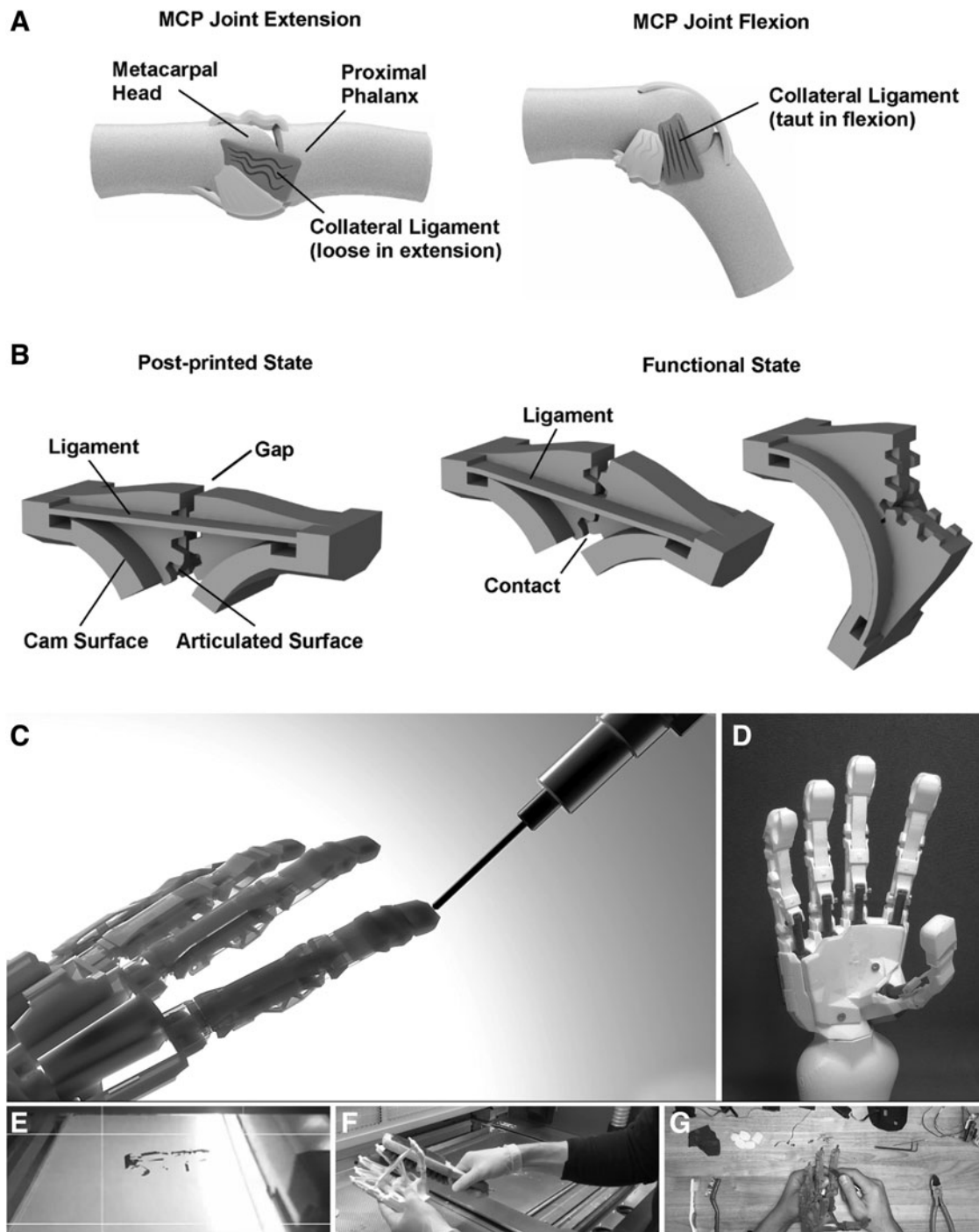
FIG. 1. Design and manufacturing process of the ST3P hand. **(A)** The anatomy and the cam effect of the human's metacarpophalangeal joint. The collateral ligament is elongated as the joint flexes. **(B)** The bio-inspired printable joint design that utilize the cam effect. The gap, the distance between the articulated surfaces, is gradually closed as the joint flexes. **(C)** A conceptual drawing that illustrates a scene in which the structure of the ST3P hand is manufactured using the single-step 3D printing process. **(D)** An actual prototype of the ST3P hand. **(E–G)** The whole manufacturing process, including 3D printing of the structure, removal of support material, and assembly for accessory components such as actuators (Supplementary Movie S1). MCP, metacarpophalangeal; ST3P, Single sTep 3D-printed Prosthetic hand.

joint angle and the design of two governing curves (i.e., the outer shape of the cam and the articulated surface) can be designed by satisfying two conditions. First, the gap at the zero joint angle must be sufficiently large for successful printing. Second, for any joint angle from the critical angle in which the state of the joint changes from one to the other, the size of the gap between articulated surfaces should be zero to provide precise flexion and extension. The parasitic motion of the joint can be restricted only when the articulated surfaces remain in contact. Thus, the designed gap starts with a
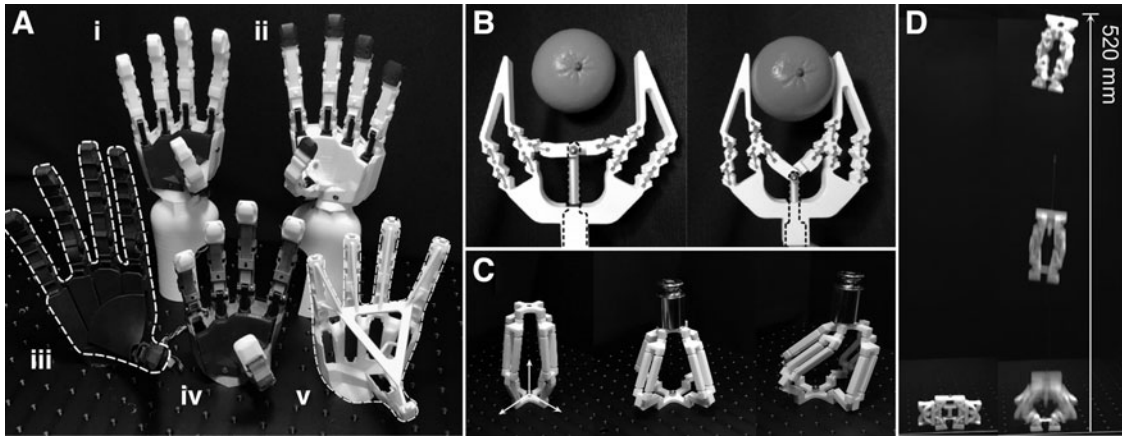
FIG. 2.   Examples of mechanisms that composed of the bio-inspired printable joints. Different 3D printing techniques and materials are used to manufacture various mechanisms to check the potential of the proposed joint design. All structures are manufactured through single-step 3D printing and actuators and electronic components were manually assembled. **(A)** Hand prototypes (i–v) for ST3P hand with different printing techniques, designs, and printing materials (iv) were manufactured using a multi-jet fusion 3D printer,[58] whereas the others were manufactured using a selective laser sintering 3D printer[55]; (iii) three joints for each finger and two joints for the thumb. Thus, the overall size of the hand is larger than the others. (v) The bridge that is designed to prevent the hand from breakage during support removal; (i) was made of PA1101 material which is relatively more flexible than PA2200,[56,57] whereas (ii), (iii), and (v) were made of PA2200 material. **(B)** A gripper with four-bar linkages and a linear actuator. Owing to limited property of available materials in FDM printing process, a desktop FDM 3D printer with a dual extruder was used to print ligaments and other parts with different materials. The ligaments are printed with a flexible filament to better prevent plastic deformation during actuation, whereas other parts, including the joints (except the ligaments), links, and support structures, are printed with a rigid filament.[72,73] **(C)** A delta robot consist of four arms and seven joints for each arm. It can deliver a 3D motion of the output platform while supporting a weight of 500 g. **(D)** A jumper mechanism with two identical legs whose joints can store and release the elastic energy. To increase elastic energy of ligaments, the jumper is made of the flexible material, PA1101. The jump height is more than six times of the jumper's body length. Demonstrations of the last three mechanisms are given in Supplementary Movie S3. FDM, fused deposition modeling.

positive value (greater than the minimum size of the printable gap) at the initial joint angle, decreases to zero as it reaches the critical angle, and remains zero from the critical angle to the maximum angle.

The size of the gap g (θ) at the joint angle θ can be expressed as a function of the geometric features, including the ligament and cam articulated surfaces [Eq. (1)], where L is the length of the ligament and C_c and C_a are the parametric representations of the curve of the cam and articulated surface, respectively. A schematic of the joint design is given in Figure 5A. Equations (2) and (3) represent the conditions required for the gap. The joint angle in the functional state, θ_f, ranges from the critical angle θ_c, to the maximum angle θ_m. The g_P is the minimum printable gap size.

$$g(\theta) = L - 2\left(\left| \overrightarrow{C_a} - \overrightarrow{C_c} \right| + \int_0^{\frac{\theta}{2}} \overrightarrow{C_c}'(t)dt \right) \quad (1)$$

$$g(0) \geq g_P \quad (2)$$

$$g(\theta_f) = 0, \quad \text{where } \theta_f \in (\theta_c, \theta_m). \quad (3)$$

To obtain a detailed design of the joint that satisfies the aforementioned conditions, we introduce an involute curve to generate the design of the articulated surfaces. The involute articulated surface ensures that the joint always has a certain gap size, thereby simplifying the joint design problem.[61]

Based on the characteristics of the involute curve, the design of the appropriate gap, articulated, and cam surfaces is derived, as given in Figure 3. First, the articulated surface was designed as an involute of the cam surface and a taut strap was fixed to the cam surface at one end and to the ground at the other end. The cam surface was designed as a circle with radius to simplify the joint design. The mathematical property of an involute curve ensures that the articulated surface is always in contact with the ground, regardless of the rotation of the structure. Second, by reflecting such a structure through a plane, a design of a symmetrical structure connected by a strap is obtained. Because each articulated surface meets the plane of symmetry, the two articulated surfaces are in contact with each other. Both the left and right structures had independent rotational degrees of freedom. The gear teeth were designed along articulated surfaces to prevent slippage (Supplementary Fig. S1). The joint design was completed by assigning an appropriate thickness to the strap and cutting a certain portion of the articulated surface such that there was a sufficient initial gap between the articulated surfaces. Detailed analyses of the design parameters, particularly the range of motion of the joint, and the design of the joint to be used in the ST3P hand can be found in Supplementary Note S3, Supplementary Figures S6 and S7.

Ligament design

The ligament is a part of the joint that undergoes elastic deformation during joint motion. The ligament is a beam
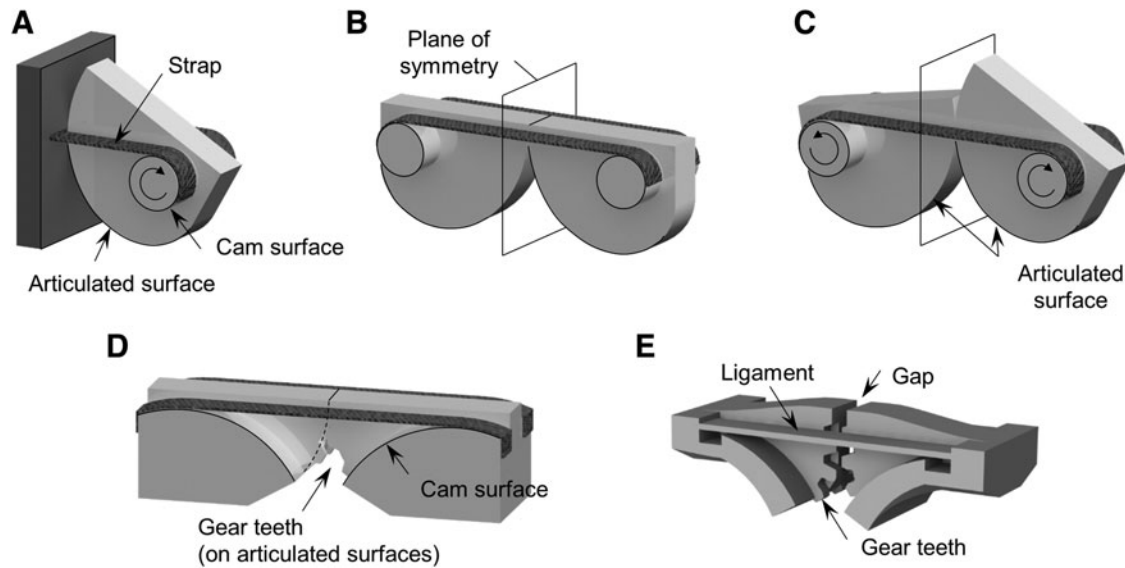
FIG. 3. Bio-inspired printable joint concept. The design of the joint is derived based on the characteristics of the involute curve. **(A)** The articulated surface is an involute of the cam surface, and the strap is attached to the ground and the cam surface. This geometrical design always ensures that the articulated surface continues to be in contact with the ground as the structure rotates. **(B)** A symmetrical structure is generated by mirroring the structure in **(A)**. **(C)** Although the structure on each side rotates independently, the contact between the two articulated surfaces is always maintained. **(D)** Gear teeth are constructed along the articulated surfaces to prevent slipping between articulated surfaces. **(E)** By cutting a part of the articulated surface, a gap is applied between the articulated surfaces.

shape with a rectangular cross-section of thickness t, width w, and length L. Among the parameters, we focused on investigating the appropriate ligament thickness because it significantly affects the joint robustness against external loads and durability during repeated use. Thin ligaments cannot withstand large external loads and are more likely to fracture when interacting with the environment. Conversely, thick ligaments may undergo plastic deformation during bending and may degrade after repeated flexion motions. Changes in width and length also influence the deformation behavior of ligaments, but the design space of these parameters is relatively narrow compared with the case of thickness.

The length is determined according to the design of the gap and articulated surfaces, and the width of the ligament is given as large as possible, considering the width of the actual human finger. Through mechanical model-based analysis (Supplementary Note S1) and experiments, the ligament thickness was designed to be 0.45 mm. The final design of the joint for the ST3P hand has a ligament of 0.45 mm thick and 20.94 mm long, an initial gap of 0.28 mm, a joint height of 5 mm, and a maximum joint angle of 120°.

Design of the ST3P hand

As a representative example of a single-step 3D printable mechanism using bio-inspired printable joints, the ST3P hand was designed (Fig. 4 and Table 1). The primary goal of the design is to (1) replicate the fundamental structures and essential functions of the human hand[62,63] while (2) allow the entire structure, including tendons and sheaths, to be 3D printed in a single step (Supplementary Fig. S4 and Supplementary Note S2). The hand structure is designed by arranging nine bio-inspired printable joints at positions where

general human finger joints are located and joining them with rigid links that have the appearance of phalanges and a palm (Supplementary Fig. S2).[64] Each finger has two bio-inspired printable joints at the place of the MCP joint and proximal interphalangeal (PIP) joint. To simplify the design, the distal interphalangeal joints are omitted. The interphalangeal and carpometacarpal joints of the thumb are also omitted; thus, the thumb has one bio-inspired printable joint for flexion and extension.

Five commercially available linear actuators were implemented at the palm of the hand, each of which drives both the MCP and PIP joints of the fingers or thumb joint. The actuators were position controlled using a microcontroller board housed on the dorsal side of the hand. For intention detection, a surface electromyography sensor detects the muscle activity of a user from the arm stump.[65] The Morse code-like patterns of the sensor signal were used as triggers to select a desired one from multiple preset grasping postures (Supplementary Fig. S5). A small display was installed on the board to allow the user to check the status of the system. To improve the grasping ability of the hand, soft fingertips and palm pads were separately manufactured and assembled on the hand.

3D printing of the ST3P hand

The entire ST3P hand structure, including the fingers, tendons, and palm, was manufactured using a single-step 3D printing process (Figs. 2A and 4). A wide range of combinations of 3D printers and printing materials has been used to build hand structures. We have figured out that selective laser sintering and multi-jet fusion 3D printing processes with their nylon-based materials are best suited for creating a joint.[66–75] These combinations produce satisfactory printing results
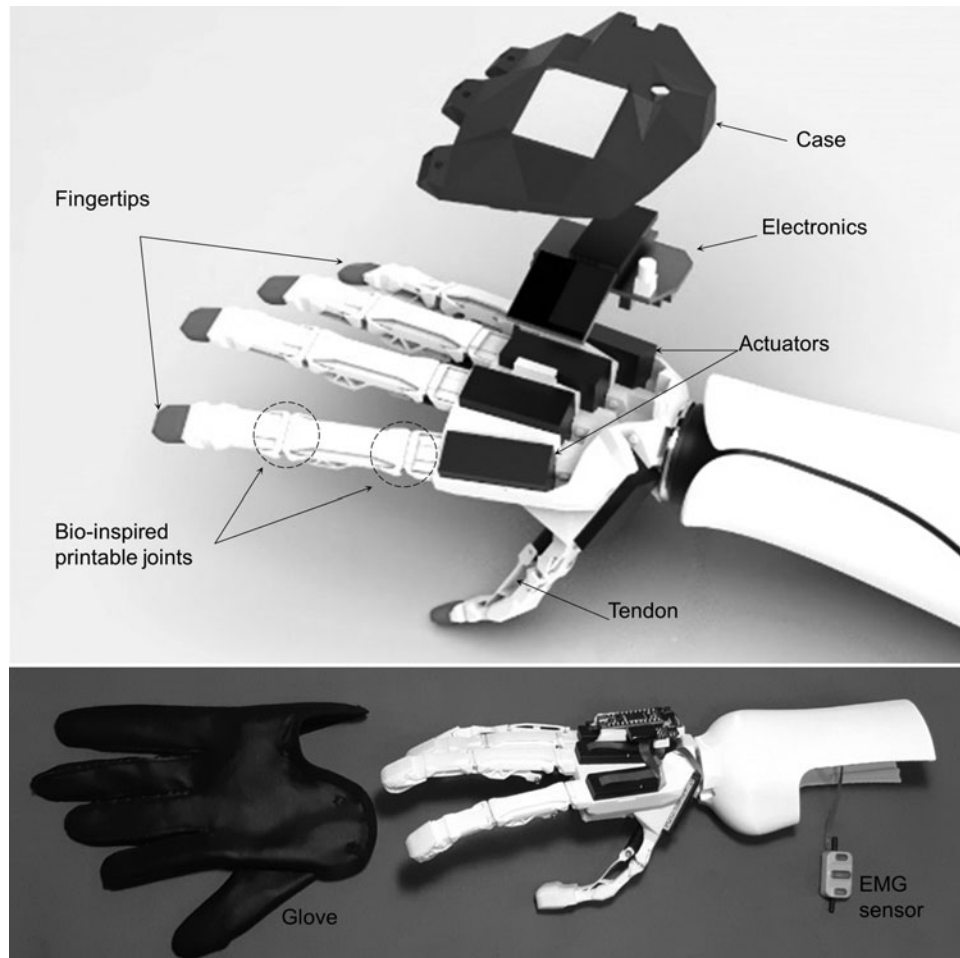
FIG. 4.   Overall design of the ST3P hand. The entire ST3P hand structure, including the fingers, tendons, and palm, was manufactured using a single-step 3D printing process. Actuators, a microcontroller board (including a small display), and a case are assembled on the dorsal side of the hand. Tendons are attached to the actuators using screws. The fingertips and palm pad (not shown) were separately printed using an FDM printer with thermoplastic polyurethane filament, and assembled. The fabric glove was designed and fabricated with two separate pieces, one for thumb and the other for rest of the hand, so that it is easy to fit into the 3D-printed hand structure. Forearm sleeve and a surface EMG sensor are also integrated into the ST3P hand. EMG, electromyography.

TABLE 1. MECHANICAL DESIGN PARAMETERS
FOR THE ST3P HAND

Item	Specifications
Size (mm)	Length × width × height: 185 × 87 × 34
Range of motion of a joint (degrees)	120
Weight (g)	255
No. of joints	9
No. of actuators	5
Max grasping force (N)	20
Max pulling force (N)	48
Time for grasping (s)	1.6
Assembly time (min)	∼6
Cost ($)	∼500
Actuator	
Max stroke (mm)	20
Max speed (mm/s)	10
Max force (N)	50
Gear ratio	100:1

ST3P, Single sTep 3D-printed Prosthetic hand.

with a high elastic modulus and strain at yield, which is favorable for the articulated surface and ligament of the joint, respectively (Supplementary Fig. S3).

Results and Discussion

Fracture moments and repeatability of the joint

Fracture, bending, and cyclic loading tests were conducted to verify the effects of the different joint ligament thicknesses. Joints of 20 different thicknesses were designed, and three specimens were fabricated for each joint design. The thickness ranges from 0.15 to 1.45 mm, and was set at 0.01 mm intervals from 0.15 to 0.20 mm, 0.05 mm intervals from 0.20 to 0.35 mm, and 0.10 mm intervals from 0.35 to 1.45 mm. Fracture and bending tests were conducted only for the joints that were successfully printed (Fig. 5B). In the fracture test, external moments were applied to the joints in the frontal, lateral, and torsional directions. By gradually increasing the magnitude of the applied moment, the occurrence of ligament fracture was observed,
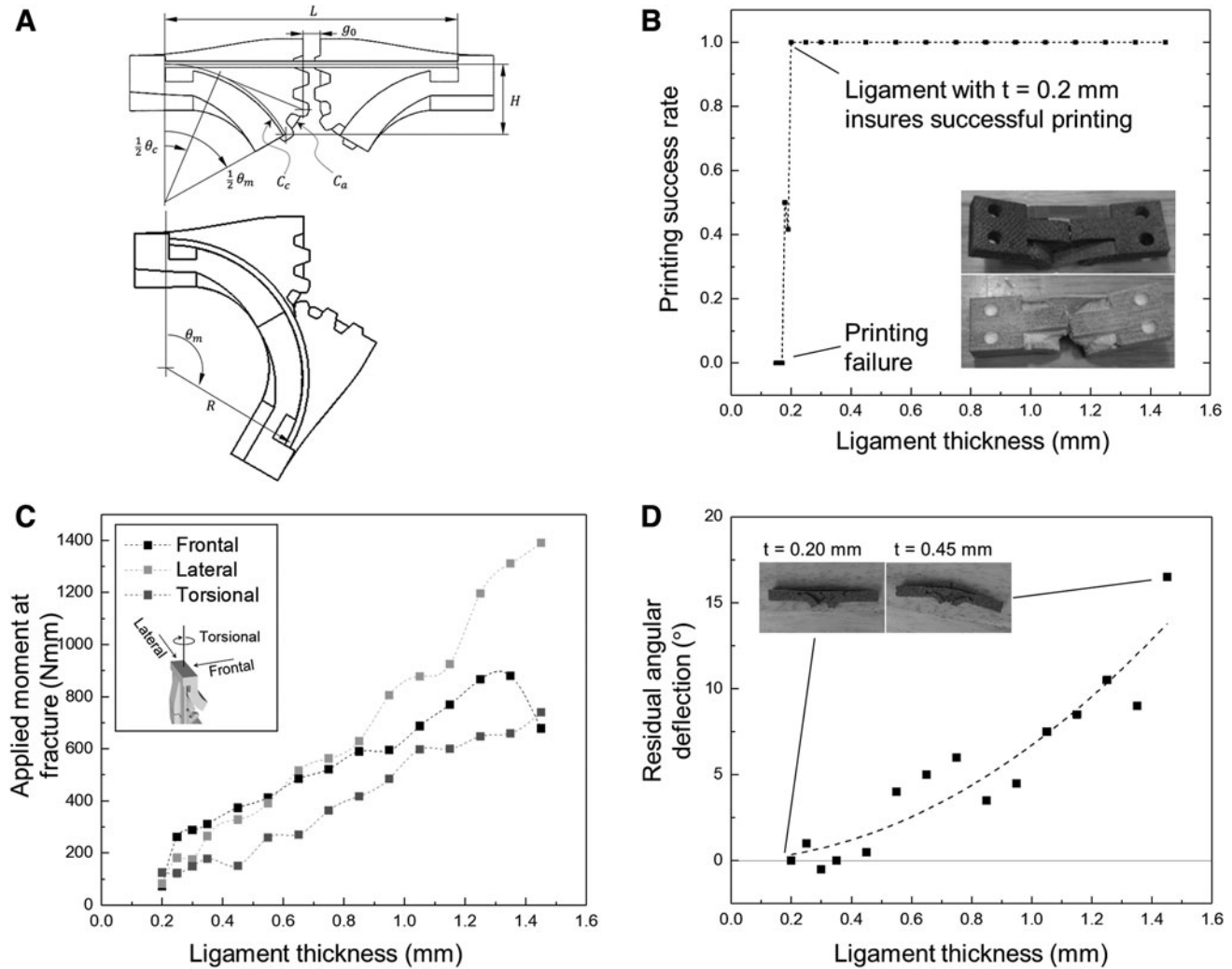
FIG. 5. Bio-inspired printable joint characteristics. **(A)** The schematic design with design parameters of a bio-inspired printable joint (L: length of ligament, H: height of joint, R: radius of the curve of cam surface). **(B)** 3D printing success rate with different ligament thicknesses. Ten joint specimens for each ligament thickness were printed and the number of print successes was counted. When the thickness is <0.2 mm, most of the joints could not be printed successfully, and incomplete ligament formation was observed. The pictures in the figure show the failures. **(C)** Applied moment at fracture and **(D)** residual deflection of joints with different ligament thicknesses. The angular deflection is calculated as the difference in joint angles before and after bending.

and the magnitude of the moment was measured. This was performed five times for the same ligament thickness and direction. Figure 5C shows the results. Joints with thicker ligaments withstood greater external moments in the frontal and lateral directions. The ligament thickness has a greater impact on the moment in the lateral direction than in the frontal direction; the joint with 1.20 mm thick ligament endures ~3.2 times the moment in the lateral direction compared with that of the 0.45 mm thick ligament joint.

A bending test was also performed to verify the repeatability of the joint. In the case of a joint in which the ligament is not sufficiently thin, plastic deformation may occur even with a small number of repeated bending. Primary tests were conducted in advance to filter out these cases. For the test, the joint was flexed to a maximum bending angle of 120°, released, and the joint angle was measured. As a result, it can be seen that the residual angle deflection of the joint whose

thickness exceeds 0.45 mm is >1° (Fig. 5D). That is, when the residual deflection of 1° is the failure threshold, the maximum ligament thickness without plastic deformation is ~0.45 mm. To investigate long-term repeatability, a cyclic loading test for the joint with 0.45 mm thick ligament was also performed. While imparting periodic flexion-extension motion to the joint, the point at which ligament fractures occurred and the number of cycles at that point were measured. Testing continued until the joint fractured or the number of cycles reached 50,000. It was checked whether the joint features including the gear teeth and ligament had a visually identifiable level of wear (Supplementary Fig. S8). As a result, no significant wear on gear teeth were observed on the joints after 50,000 cycles loading and unloading other than minor scratches on the gear teeth. In addition, to understand the effect of cyclic loading on the ligament, the fracture characteristics of the ligament during the test were

TABLE 2. SPECIFICATION COMPARISON OF 3D-PRINTED PROSTHETIC HANDS

Item	ST3P hand (proposed)	Brunel hand 2.0	Cyborg Beast hand
No. of joints	9	9	11 (including wrist joint)
No. of actuators	5	4	—
No. of mechanical components	10	37	22
Primary components (joints, phalanges, tendons, palm)	2	37	22
Secondary components (e.g., fingertips, palm pad, glove)	8	Not specified	Not specified
Actuation methods	Linear actuators and 3D-printed tendons	Flexion by tendons and linear actuators. Passive extension by elastic force	Body-powered prosthetics actuated by wrist movement

Fixing elements such as bolts/nuts or screws are excluded when counting the number of mechanical components.

also investigated. The result showed that the yield moment of joint specimens decreased ∼10%, from 413.3 to 368.3 Nmm, after 50,000 cycles of loading.

Easiness of assembly

Replacing traditional multipart prosthetic joints with bio-inspired printable joints remarkably reduces the total number of parts required for the hand and simplifies the hand assembly. To quantitatively evaluate the simplicity of the assembly, the assembly time for the ST3P hand was compared with that of other well-known 3D-printed prosthetic hands, including the Brunel hand 2.0 and Cyborg Beast hand.[38,39] These prosthetic hands were chosen because they have comparable specifications with the ST3P hand (Table 2). Each hand was assembled according to the instructions provided by the developers. An experimenter performed the assemblies with sufficient mastery of assembly through repeated prepractice, and the average assembly time for each hand was obtained by repeating the assembly process three times.

Figure 6A and B provides the assembly processes of the hands and the resultant assembly times. Brunel Hand 2.0 is fabricated by mounting motors on the palm of the hand and then assembling wire tendons and finger joints. The Cyborg Beast hand was fabricated by assembling finger joints, passive extender wire tendons, and flexor wire tendons. On the contrary, the assembly process of the ST3P hand involved only a few steps: attaching linear actuators and electronics and connecting the power source (Supplementary Movie S1). The assembly took ∼6 min, only one-tenth of the other prosthetics. The total production time to create a single ST3P hand for one operator using a single 3D-printer[58] was estimated to be ∼86 min (80 min for printing and support removal, 6 min for assembly). This efficient manufacturing and assembly process allowed us to rapidly create many prototypes of the ST3P hand with various designs (Fig. 2A).

Hand grasping performance

The final design of the ST3P hand has similar kinematics to those of the human hand, enabling the hand to perform basic tasks for ADLs. The primary ADL task of the hand is to grasp

and hold an object with sufficient force using all fingers and thumbs. To demonstrate the grasping performance, sensor-embedded dummy objects and several daily life items (baseball, card, cylindrical box, bowl, plastic bottle, and laptop bag) were used. The dummy object included a rectangular box with a height of 10 mm, a small cylinder with a diameter of 55 mm, a large cylinder with a diameter of 90 mm, and a spherical ball with a diameter of 55 mm. During the ST3P hand grasping of these objects, the pulling force or grasp strength was measured by the embedded load cells. The measured pulling force was 48 N and the grasp strengths was 20 N approximately (Fig. 6C). Grip strength tends to vary considerably depending on the size and shape of the object, owing to the lack of appropriate force feedback control. Figure 6D and Supplementary Movie S2 show that ST3P can take various postures, hold daily items, and interact with the environment (e.g., writing on a tablet using a pen).

Single-step printability and versatility

We have demonstrated that by single-step printing of the ST3P hand, the benefits of 3D printing can be extended from a set of static objects to movable, functional mechanisms. Provided that a 3D printer is available, ST3P hand design can be easily manufactured without specialized skill sets or knowledge. Designers can easily realize customized conceptual designs into physical replications, accelerating the process of design iterations or updates. Prosthetic users can have multiple variations of affordable prosthetic hands that fit their purpose of use, with different esthetics and functionalities, such as housework or sports. Indeed, the concept of single-step 3D printing using bio-inspired printable joints is not limited to prostheses and can be applied to different robotic mechanisms. To explore the potential of single-step 3D printing, three mechanisms, delta, gripper, and jumping mechanism, were designed by integrating bio-inspired printable joints (Fig. 2B–D).[76] Because the bio-inspired printable joint design can minimize the joint gap, unlike other 3D printable joints, a delta mechanism is expected to exhibit an acceptable degree of precision without gap-caused positional errors. The gripper was proposed to explore the compatibility of the proposed joint with a fused deposition modeling-based printing method. The jumper
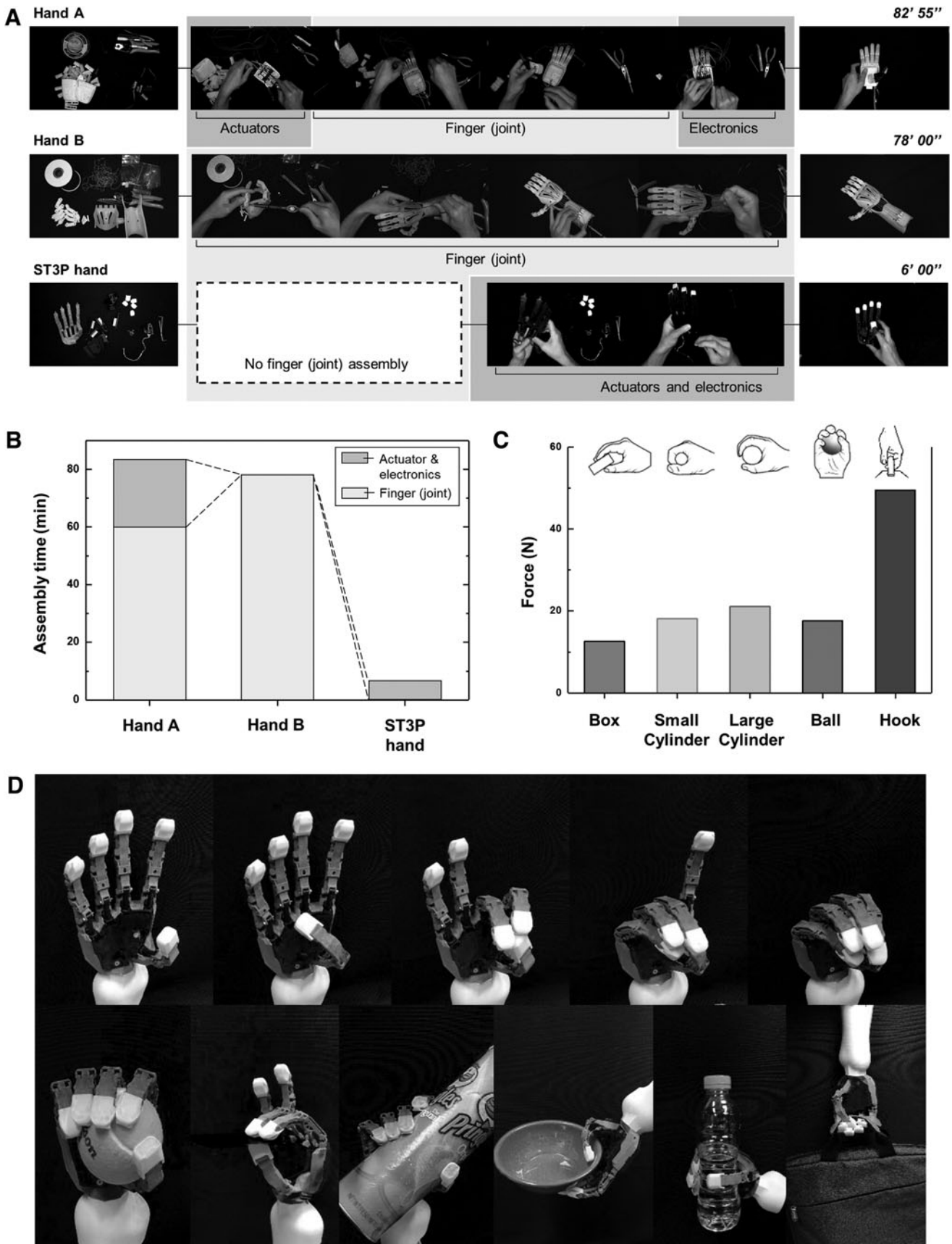
FIG. 6. Performance of the ST3P hand. **(A)** Assembly processes for the three different prosthetic hands, including the Brunel hand 2.0 (marked as hand A), Cyborg Beast hand (marked as hand B), and ST3P hand. The ST3P hand was assembled by integrating linear actuators and the electronics without the need for integrating finger joints and tendons. **(B)** Comparison result for the assembly time of the ST3P hand with other 3D-printed prosthetic hands. **(C)** The measured grasp strength for different objects and measured pulling force of the ST3P hand. **(D)** Gestures and grasping motions that can be performed by the ST3P hand.

9

was designed with the use of the joint as an energy storage and release element. The feasibility of each mechanism was tested, as given in Figure 2 and Supplementary Movie S3. Detailed designs of the mechanisms are given in Supplementary Note S4.

Conclusion

We developed a bio-inspired printable joint that resolves the typical problem of 3D printed joints. The existing 3D printing methods cannot directly produce tightly mated pins and holes. Therefore, to create a 3D-printed joint, it is necessary to assemble the joint parts after printing them separately or to print a joint with a gap between the pin and hole. The cam effect, inspired by the human MCP joint, enables the achievement of a zero gap between moving surfaces after 3D printing. The joint geometries were designed to close the gap when the joint was flexed. Contact at the gap makes it possible for the joint to generate precise motion.

The bio-inspired printable joint can save the time and labor costs required to manufacture robotic mechanisms. Facilitated manufacturing can accelerate the iterative design process and help developers quickly obtain an optimized design. As a proof-of-concept, an ST3P hand with bio-inspired printable finger joints was designed and demonstrated. This joint design enabled the structure of the ST3P hand to be manufactured without assembly. The ST3P hand is lightweight (~ 255 g), low-cost, and has a kinematic design similar to that of a human hand, which is advantageous for performing hand-related tasks. Although the ST3P hand has been tested only in a laboratory environment, we will continue to develop the ST3P hand by conducting experiments with hand amputees in the near future. We hope that the development of the ST3P hand will be a step toward the future when all hand amputees will have an ideal (customized, affordable, lightweight, and fully functional) robotic hand prosthesis. Advanced 3D printing technologies, such as multimaterial 3D printing or printing with smart materials,[77–79] have the potential to improve the performance and create new functionalities. Although the proposed work provides a proof of concept for single-step 3D printing mechanisms, the eventual development of entire libraries on single-step 3D printable robotics components, including actuators and sensors,[80–88] could revolutionize the robotic industry by enabling fully automated robotic system manufacturing.

Authors' Contributions

H.L.: Conceptualization (lead); methodology (lead); validation (supporting); visualization (lead); writing—original draft (equal). J.P.: Data curation (lead); methodology (supporting); validation (lead); writing—original draft (equal). B.B.K.: Conceptualization (supporting); data curation (supporting); validation (supporting); writing—original draft (equal). K.-J.C.: Project administration (lead); supervision (lead).

Acknowledgments

The authors thank C.W. Bundschu for revising the article and J.J.-R. Song for working on the graphical presentation of the figures.

Supplementary Material

Supplementary Figure S1
Supplementary Figure S2
Supplementary Figure S3
Supplementary Figure S4
Supplementary Figure S5
Supplementary Figure S6
Supplementary Figure S7
Supplementary Figure S8
Supplementary Note S1
Supplementary Note S2
Supplementary Note S3
Supplementary Note S4
Supplementary Movie S1
Supplementary Movie S2
Supplementary Movie S3

References

1. Cuellar JS, Plettenburg D, Zadpoor AA, et al. Design of a 3D-printed hand prosthesis featuring articulated bio-inspired fingers. Proc Inst Mech Eng H 2021;235(3):336–345.
2. Lu H, Zou Z, Wu X, et al. Biomimetic prosthetic hand enabled by liquid crystal elastomer tendons. Micromachines 2021;12(7):736; doi: 10.3390/mi12070736.
3. Xu Z, Todorov E. Design of a highly biomimetic anthropomorphic robotic hand towards artificial limb regeneration. IEEE Int Conf Robot Autom 2016; Stockholm, Sweden. New York: IEEE.
4. Deshpande AD, Xu Z, Weghe MJ, et al. Mechanisms of the anatomically correct testbed hand. IEEE ASME Trans Mechatron 2011;18(1):238–250; doi: 10.1109/TMECH.20 11.2166801.
5. Abd MA, Paul R, Aravelli A, et al. Hierarchical tactile sensation integration from prosthetic fingertips enables multi-texture surface recognition. Sensors 2021;21(13): 4324; doi: 10.3390/s21134324.
6. Nguyen AT, Xu J, Jiang M, et al. A bioelectric neural interface towards intuitive prosthetic control for amputees. J Neural Eng 2020;17(6):066001; doi: 10.1088/1741-2552/ abc3d3
7. Gardner M, Mancero Castillo CS, Wilson S, et al. A multimodal intention detection sensor suite for shared autonomy of upper-limb robotic prostheses. Sensors 2020;20(21):6097; doi: 10.3390/s20216097.
8. Parajuli N, Sreenivasan N, Bifulco P, et al. Real-time EMG based pattern recognition control for hand prostheses: A

review on existing methods, challenges and future implementation. Sensors 2019;19(20):4596; doi: 10.3390/s19204596.

9. Raspopovic S, Valle G, Petrini FM. Sensory feedback for limb prostheses in amputees. Nat Mater 2021;20(7):925–939; doi: 10.1038/s41563-021-00966-9.

10. Gu G, Zhang N, Xu H, et al. A soft neuroprosthetic hand providing simultaneous myoelectric control and tactile feedback. Nat Biomed Eng 2021; doi: 10.1038/s41551-021-00767-0.

11. Simons MF, Digumarti KM, Le NH, et al. B:Ionic glove: A soft smart wearable sensory feedback device for upper limb robotic prostheses. IEEE Robot Autom Lett 2021;6(2):3311–3316; doi: 10.1109/LRA.2021.3064269.

12. Belter JT, Segil JL, SM B. Mechanical design and performance specifications of anthropomorphic prosthetic hands: A review. J Rehabil Res Dev 2013;50(5):599; doi: 10.1682/JRRD.2011.10.0188.

13. Bebionic hand, Ottobock. Available from: https://www.ottobockus.com/prosthetics/upper-limb-prosthetics/solution-overview/bebionic-hand [Last accessed: April 18, 2022].

14. i-Limb Ultra, Ossur. Available from: https://www.ossur.com/en-gb/prosthetics/arms/i-limb-ultra [Last accessed: April 18, 2022].

15. Carey SL, Lura DJ, Highsmith MJ. Differences in myoelectric and body-powered upper-limb prostheses: Systematic literature review. J Rehabil Res Dev 2015;52(3):247–262; doi: 10.1682/JRRD.2014.08.0192.

16. Godfrey SB, Rossi M, Piazza C, et al. SoftHand at the CYBATHLON: A user's experience. J Neuroeng Rehabil 2017;14(1):124; doi: 10.1186/s12984-017-0334-y.

17. Maker Hand. The Most Functional Prosthetic hand in the world. Available from: https://www.makerhand.com [Last accessed: April 18, 2022].

18. Cybathlon. Cybathlon 2020 Global Edition Livestream. Available from: https://cybathlon.ethz.ch/en/projects-events/edition/cybathlon-2020 [Last accessed: April 18, 2022].

19. Biddiss EA, Chau TT. Upper limb prosthesis use and abandonment: A survey of the last 25 years. Prosthet Orthot Int 2007;31(3):236–257; doi: 10.1080/03093640600994581.

20. Lotti F, Vassura G. A novel approach to mechanical design of articulated fingers for robotic hands. IEEE Int Conf Intell Robots Syst 2002; Lausanne, Switzerland. New York: IEEE. 2:1687–1692.

21. Hughes JA, Maiolino P, Iida F. An anthropomorphic soft skeleton hand exploiting conditional models for piano playing. Sci Robot 2018;3(25):eaau3098; doi: 10.1126/scirobotics.aau3098.

22. Catalano MG, Grioli G, Farnioli E, et al. Adaptive synergies for the design and control of the Pisa/IIT SoftHand. Int J Rob Res 2014;33(5):768–782; doi: 10.1177/0278364913 51899.

23. Tawk C, Zhou H, Sariyildiz E, et al. Design, modeling, and control of a 3D printed monolithic soft robotic finger with embedded pneumatic sensing chambers. IEEE ASME Trans Mechatron 2020;26(2):876–887; doi: 10.1109/TMECH.2020.3009365.

24. Manti M, Hassan T, Passetti G, et al. A bioinspired soft robotic gripper for adaptable and effective grasping. Soft Robot 2015;2(3):107–116; doi: 10.1089/soro.2015.0009.

25. Dollar AM, Howe RD. The SDM hand as a prosthetic terminal device: A feasibility study. In: IEEE International Conference on Rehabilitation Robotics. 2007; Noordwijk, Netherlands. New York: IEEE. pp. 978–983.

26. Dollar AM, Howe RD. The highly adaptive SDM hand: Design and performance evaluation. Int J Rob Res 2010;29(5):585–597; doi: 10.1177/0278364909360852.

27. Ma RR, Odhner LU, Dollar AM. A modular, open-source 3D printed underactuated hand. In: IEEE International Conference on Robotics and Automation. 2013: Karlsruhe, Germany. New York: IEEE. pp. 2737–2743.

28. Odhner LU, Jentoft LP, Claffee MR, et al. A compliant, underactuated hand for robust manipulation. Int J Rob Res 2014;33(5):736–752; doi: 10.1177/0278364913514466.

29. Carrozza MC, Cappiello G, Stellin G, et al. A cosmetic prosthetic hand with tendon driven under-actuated mechanism and compliant joints: Ongoing research and preliminary results. In: International Conference on Robotics and Automation. 2005; Barcelona, Spain. New York: IEEE. pp. 2661–2666.

30. Deimel R, Brock O. A novel type of compliant and underactuated robotic hand for dexterous grasping. Int J Rob Res 2016;35(1–3):161–185; doi: 10.1177/027836491 5592961.

31. Montierth JR, Todd RH, Howell LL. Analysis of elliptical rolling contact joints in compression. J Mech Des 2011;133(3):031001; doi: 10.1115/1.4003499.

32. Guérinot AE, Magleby SP, Howell LL, et al. Compliant joint design principles for high compressive load situations. J Mech Des 2005;127(4):774–781; doi: 10.1115/1.1862677.

33. Mavroidis C, DeLaurentis KJ, Won J, et al. Fabrication of non-assembly mechanisms and robotic systems using rapid prototyping. J Mech Des 2001;123(4):516–524; doi: 10.1115/1.1415034.

34. Lussenburg K, Sakes A, Breedveld P. Design of non-assembly mechanisms: A state-of-the-art review. Addit Manuf 2021;39:101846.

35. Cuellar JS, Smit G, Plettenburg D, et al. Additive manufacturing of non-assembly mechanisms. Addit Manuf 2018;21:150–158; doi: 10.1016/j.addma.2018.02.004.

36. Calì J, Calian DA, Amati C, et al. 3D-printing of non-assembly, articulated models. ACM Trans Graph 2012;31(6):1–8; doi: 10.1145/2366145.2366149.

37. Ten Kate J, Smit G, Breedveld P. 3D-printed upper limb prostheses: A review. Disabil Rehabil Assist Technol 2017;12(3):300–314; doi: 10.1080/17483107.2016.1253117.

38. Brunel Hand 2.0., Open Bionics. Available from: https://openbionicslabs.com [Last accessed: April 18, 2022].

39. Zuniga J, Katsavelis D, Peck J, et al. Cyborg beast: A low-cost 3d-printed prosthetic hand for children with upper-limb differences. BMC Res Notes 2015;8:10; doi: 10.1186/s13104-015-0971-9.

40. Wei X, Tian Y, Joneja A. A study on revolute joints in 3D-printed non-assembly mechanisms. Rapid Prototyp J 2016;22(6):901–933; doi: 10.1108/RPJ-10-2014-0146.

41. Chen Y, Zhezheng C. Joint analysis in rapid fabrication of non-assembly mechanisms. Rapid Prototyp J 2011;17(6):408–417; doi: 10.1108/13552541111184134.

42. Flores P, Ambrósio J. Revolute joints with clearance in multibody systems. Comput Struct 2004;82(17–19):1359–1369; doi: 10.1016/j.compstruc.2004.03.031.

43. Li-Xin X, Yong-Gang L. Investigation of joint clearance effects on the dynamic performance of a planar 2-DOF pick-and-place parallel manipulator. Robot Comput Integr Manuf 2014;30(1):62–73; doi: 10.1016/j.rcim.2013.09.002.

44. Li X, Ding X, Chirikjian GS. Analysis of angular-error uncertainty in planar multiple-loop structures with joint clearances. Mech Mach Theory 2015;91:69–85; doi: 10.1016/j.mechmachtheory.2015.04.005.

45. Rajagopalan S, Cutkosky M. Error analysis for the in-situ fabrication of mechanisms. J Mech Des 2003;125(4):809–822; doi: 10.1115/1.1631577.

46. Liu Y, Zhang J, Yang Y, et al. Study on the influence of process parameters on the clearance feature in non-assembly mechanism manufactured by selective laser melting. J Manuf Process 2017;27:98–107; doi: 10.1016/j.jmapro.2017.04.005.

47. Adam GA, Zimmer D. Design for additive manufacturing—Element transitions and aggregated structures. CIRP J Manuf Sci Technol 2014;7(1):20–28; doi: 10.1016/j.cirpj.2013.10.001.

48. Su X, Yang Y, Wang D, et al. Digital assembly and direct fabrication of mechanism based on selective laser melting. Rapid Prototyp J 2013;90(3):166–172; doi: 10.1108/13552541311312157

49. Lipson H, Moon FC, Hai J, et al. 3-D printing the history of mechanisms. J Mech Des 2005;127(5):1029–1033; doi: 10.1088/1748-3190/10/5/055003.

50. Yang Y, Wang D, Su X, et al. Design and rapid fabrication of non-assembly mechanisms. In: IEEE Int Conf Manuf Autom. 2010. Hong Kong, China. New York: IEEE. pp. 61–63.

51. Jansen B, Doubrovski EL, Verlinden JC. Animaris Geneticus Parvus: Design of a complex multi-body walking mechanism. Rapid Prototyp J 2014;20(4):311–319.

52. Song C, Yang Y, Xiao Z, et al. Design and direct manufacture of non-assembly abacus by selective laser melting. In: International Symposium on Optoelectronic Technology and Application; doi: 10.1117/12.2072609.

53. Calignano F, Manfredi D, Ambrosio EP, et al. Direct fabrication of joints based on direct metal laser sintering in aluminum and titanium alloys. Procedia CIRP 2014;21: 129–132.

54. Crescenzio FD, Lucchi F. In: Advances on Mechanics, Design Engineering and Manufacturing. Lecture Notes in Mechanical Engineering. (Eynard B, Nigrelli V, Oliveri S, et al. eds.) Springer, Cham: Switzerland; 2017; doi: 10.1007/978-3-319-45781-9_26.

55. Li X, Zhao J, He R, et al. Parametric design of scalable mechanisms for additive manufacturing. J Mech Des 2018;140(2):022302; doi: 10.1115/1.4038300.

56. Chen Y, Lu J. Minimise joint clearance in rapid fabrication of non-assembly mechanisms. Int J Comput Integr Manuf 2011;24(8):726–734; doi: 10.1108/13552541311312157.

57. Song X, Chen Y. Joint design for 3-D printing non-assembly mechanisms. In: Proceedings of the ASME International Design Engineering Technical Conferences. 2012; doi: 10.1115/DETC2012-71528.

58. Schultz RJ, Storace A, Krishnamurthy S. Metacarpophalangeal joint motion and the role of the collateral ligaments. Int Orthop 1987;11(2):149–155; doi: 10.1007/BF00266701.

59. Neumann DA. Kinesiology of the Musculoskeletal System: Foundation for rehabilitation. 2nd ed. Mosby/Elsevier: St. Louis, Mo.; 2010.

60. Lawry GV, Kreder HJ, Hawker G, et al. The wrist and hand. In: Fam's Musculoskeletal Examination and Joint Injection Techniques. 2nd ed. Mosby: Philadelphia; 2010; pp. 29–43.

61. Rutter JW. Geometry of Curves. 1st ed. Chapman and Hall/CRC: New York; 2000.

62. Kamper DG, Cruz EG, Siegel MP. Stereotypical fingertip trajectories during grasp. J Neurophysiol 2003;90(6):3702–3710; doi: 10.1089/3dp.2015.0039.

63. Vincent Systems. Available from:www.vincentsystems.de/?lang=en [Last accessed: April 18, 2022].

64. Result of Human hand measurements data, Size Korea. Available from: https://sizekorea.kr/human-meas-search/human-data-search/meas-item [Last accessed: April 18, 2022].

65. MyoBock electrode, Ottobock. Available from: professionals.ottobock.com.au/Products/Prosthetics/Prosthetics-Upper-Limb/Adult-Terminal-Devices/13E200-MyoBock-electrode/p/13E200 [Last accessed: April 18, 2022].

66. Formiga P 110 Velocis, EOS. Available from: https://www.eos.info/en/additive-manufacturing/3d-printing-plastic/eos-polymer-systems/formiga-p-110-velocis [Last accessed: April 18, 2022].

67. Polyamide 12 White, EOS. Available from: www.eos.info/en/additive-manufacturing/3d-printing-plastic/sls-polymer-materials/polyamide-pa-12-alumide [Last accessed: April 18, 2022].

68. Polyamide 11 Nylon, EOS. Available from: https://www.eos.info/en/additive-manufacturing/3d-printing-plastic/sls-polymer-materials/pa-11-nylon-abs-pa6 [Last accessed: April 18, 2022].

69. HP 3D jet fusion 4200, HP. Available from: https://www.hp.com/us-en/printers/3d-printers/products/multi-jet-fusion-4200.html [Last accessed: April 18, 2022].

70. HP 3D High Reusability PA 11, HP. Available from: cimquest-inc.com/resource-center/HP/Materials/HP-PA11-Datasheet.pdf [Last accessed: April 18, 2022].

71. Ultimaker Nylon TDS, Ultimaker. Available from: support.ultimaker.com/hc/en-us/articles/360011962600-Ultimaker-Nylon-TDS [Last accessed: April 18, 2022].

72. Ultimaker PLA TDS, Ultimaker. Available from: support.ultimaker.com/hc/en-us/articles/360011962720-Ultimaker-PLA-TDS [Last accessed: April 18, 2022].

73. HP 3D High Reusability PA 12, HP. Available from: https://cimquest-inc.com/resource-center/HP/Materials/HP-PA12-Datasheet.pdf [Last accessed: April 18, 2022].

74. VeroWhitePlus, Stratasys. Available from: https://www.stratasysdirect.com/wp-content/themes/stratasysdirect/files/material-datasheets/polyjet/PolyJet_VeroWhitePlus_Material_Specifications.pdf [Last accessed: April 18, 2022].

75. Alvarez-Primo F, English J, Mireles J. Appendix E: Material properties. In: Wohlers Report 2016: 3D Printing and Additive Manufacturing State of the Industry: Annual Worldwide Progress Report. Wohlers Associates; Fort Collins, Colorado; 2016. Available from: www.wohlersassociates.com/materials2016.pdf [Last accessed: April 18, 2022].

76. McClintock H, Temel FZ, Doshi N, et al. The milliDelta: A high-bandwidth, high-precision, millimeter-scale Delta robot. Sci Robot 2018;3(14):eaar3018; doi: 10.1126/scirobotics.aar3018.

77. D de Marco C, Pané S, Nelson BJ. 4D printing and robotics. Sci Robot 2018;3(18):eaau0449; doi: 10.1126/scirobotics.aau0449.

78. Choi J, Kwon OC, Jo W, et al. 4D printing technology: A review. 3D Print Addit Manuf 2015;2(4):159–167; doi: 10.1089/3dp.2015.0039.

79. Wagner M, Chen T, Shea K. Large shape transforming 4D auxetic structures. 3D Print Addit Manuf 2017;4(3):133–142; doi: 10.1089/3dp.2017.0027.

80. Bartlett NW, Tolley MT, Overvelde JT, et al. A 3D-printed, functionally graded soft robot powered by combustion. Science 2015;349(6244):161–165; doi: 10.1126/science.aab0129.

81. Peele BN, Wallin TJ, Zhao H, et al. 3D printing antagonistic systems of artificial muscle using projection stereo-

lithography. Bioinspir Biomim 2015;10(5):055003; doi: 10.1088/1748–3190/10/5/055003.

82. Niiyama R, Sun X, Sung C, et al. Pouch motors: Printable soft actuators integrated with computational design. Soft Robot 2015;2(2):59–70; doi: 10.1089/soro.2014.0023.

83. MacCurdy R, Katzschmann R, Kim Y, et al. Printable hydraulics: A method for fabricating robots by 3D co-printing solids and liquids. In: IEEE International Conference on Robotics and Automation. 2016.

84. O'Brien KW, Xu PA, Levine DJ, et al. Elastomeric passive transmission for autonomous force-velocity adaptation applied to 3D-printed prosthetics. Sci Robot 2018;3(23): eaau5543; doi: 10.1126/scirobotics.aau5543.

85. Yirmibesoglu OD, Morrow J, Walker S, et al. Direct 3D printing of silicone elastomer soft robots and their performance comparison with molded counterparts. In: IEEE International Conference on Soft Robotics. 2018. Chen T, Shea L. An autonomous programmable actuator and shape reconfigurable structures using bistability and shape memory polymers. 3D Print Addit Manuf 2018;5(2):91–101; doi: 10.1089/3dp.2017.0118.

86. Chen T, Shea L. An autonomous programmable actuator and shape reconfigurable structures using bistability and

shape memory polymers. 3D Print Addit Manuf 2018;5(2):91–101; doi: 10.1089/3dp.2017.0118.

87. Khondoker MAH, Baheri N, Sameoto D. Tendon-driven functionally gradient soft robotic gripper 3D printed with intermixed extrudate of hard and soft thermoplastics. 3D Print Addit Manuf 2019;6(4); doi: 10.1089/3dp.2018 .0102.

88. Saari M, Xia B, Cox B, et al. Fabrication and analysis of a composite 3D printed capacitive force sensor. 3D Print Addit Manuf 2016;3(3):137–141; doi: 10.1089/3dp.2016.0021.

Address correspondence to:
Kyu-Jin Cho
Biorobotics Laboratory
Department of Mechanical Engineering
Seoul National University
Gwanak-ro 1, Gwanak-gu
Seoul 08826
Republic of Korea

E-mail: kjcho@snu.ac.kr